Adaptive Transceiver Design for C-RAN in mmWave Communications

K. Satyanarayana, *Student Member, IEEE,* Mohammed El-Hajjar, *Senior Member, IEEE,* Ping-Heng Kuo, Alain Mourad, and Lajos Hanzo, *Fellow, IEEE*

***Abstract*—An adaptive array design is proposed for hybrid beamforming in millimeter wave (mmWave) communications in the context of cloud radio access networks (C-RAN). More explicitly, the adaptive design focuses on the physical layer aspect of C-RAN. The adaptation is performed at two levels, depending on whether the channel is of line-of-sight (LOS) or non-line-of-sight (NLOS) nature. Firstly, the antenna array architecture can be adapted between a fully-connected and a sub-array-connected architecture. Then, the employment of a digital precoder in the baseband is decided based on both the channel conditions and the architecture employed. We show that the proposed adaptive design performs better than the fully-connected and sub-array-connected constituent designs, when the channel varies between LOS and NLOS scenarios. Then, we extend our proposed adaptive design to mmWave communications in the context of C-RAN, where we propose an adaptive virtual cell formation algorithm, where a user can be connected to one or two remote radio heads (RRHs), depending on the channel conditions.**

***Index Terms*—Millimeter Wave, Hybrid Beamforming, MIMO, Adaptive Arrays, C-RAN, Virtual Cells.**

I. Introduction

RECENT studies show that there is an increasing demand for high data rates among the mobile users [1], hence harnessing the large bandwidth available at mmWave frequencies becomes a promising solution [2]. However, mmWave frequencies suffer from high propagation losses due to oxygen absorption, water vapor and foliage, which results in a low signal-to-noise ratio (SNR) at the receiver. Thus, to compensate for the propagation losses, typically directional transmissions are invoked, where the signal is steered in the desired direction by *beamforming* [3]. Conventionally, beamforming is performed in two ways: *analog beamforming* and *digital beamforming*. In analog beamforming, the signal is steered using phase shifters, whose disadvantage is that the angular resolution of the phase shifters is inaccurate. This inaccuracy is avoided in the case of digital beamforming, where the signals are steered digitally, but this requires dedicated digital-to-analog (DAC) and analog-to-digital (ADC) converters for each antenna. This imposes a high hardware complexity and power consumption at mmWave frequencies, since the number of antenna elements (AEs) can be on the order of a few hundred. Therefore, a hybrid beamforming based system is conceived, where analog beamforming is carried out in the RF stage, while digital beamforming is invoked at the baseband. The advantage of this hybrid design over the conventional analog or digital methods is that it provides similar performance at a reduced complexity, while the limitations of the analog beamforming are corrected by the digital beamforming [4].

The fiscal support of InterDigital and of the ERC Advanced Fellow Grant Beam-Me-Up is gratefully acknowledged.

The DOI for the assosiated dataset can be found at https://doi.org/10.5258/SOTON/D0306

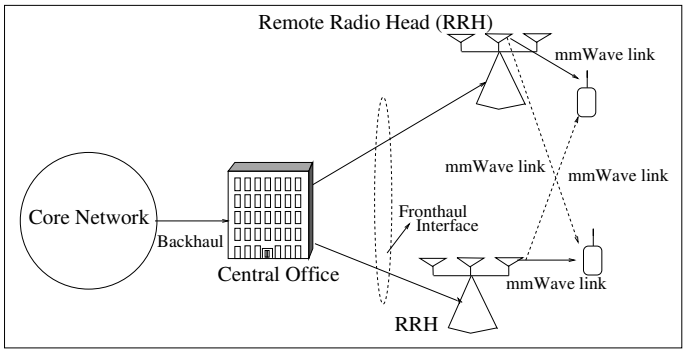

Fig. 1. C-RAN architecture.

On the other hand, to support the end-users' ever-growing need and to provide better energy efficiency, C-RAN is expected to play a major role in 5G. The main idea of C-RAN is to split the base stations into low power and low complexity remote radio heads (RRHs) coordinated by a central unit (CU) located at the central office (CO) [5] as shown in Fig. 1. This relies on using fronthaul links that connect the RRHs to the CU, with the aid of diverse transmission media that includes fiber-optic cable, digital subscriber lines (DSL), or wireless mmWave channels, as shown in Fig. 1. In C-RAN, the centralized/joint signal processing of RRHs is carried out at the CO by the CU, which makes the architecture both cost-effective and energy-efficient [5]. This makes the C-RAN an attractive choice for network densification [6].

Combining the idea of hybrid beamforming system for mmWave in the physical (PHY) layer of C-RAN can provide many benefits in terms of cost and capacity by harnessing the large bandwidth at mmWave frequencies. Traditionally, in mmWave, different hybrid beamforming designs have been described in [7], namely fully-connected design and array of sub-array-connected design (ASA). In the fully-connected design, the phase shifters of each RF chain are connected to all antennas, while in the ASA design, the phase shifters of each RF chain are connected to only a subset of antennas. Since the number of phase shifters employed in the ASA is lower than those employed in the fully-connected design, it is more power efficient [8]. Furthermore, the distributed nature of C-RAN can be seen as an extension of the ASA, i.e. when only one RRH is used, it is analogous to fully-connected design, and when more than one RRH is used, it is analogous to the ASA design, where each sub-array maybe fully-connected.

In the literature, different adaptive system designs were conceived. Yilmaz *et. al* [9] advocated a spatially reconfig-

urable adaptive array, while Song *et. al* [10] proposed an adaptive beam alignment for dual-polarized MIMO systems. The so-called Doppler resilient adaptive angle-of-arrival estimation and beamforming algorithms were discussed in [11] and adaptive compressed sensing based channel estimation was advocated by Alkhateeb *et. al* in [12]. El-Hajjar *et. al* [13] proposed a near-instantaneous adaptive scheme subject to rapidly-fluctuating time-variant channels.

On the other hand, for PHY layer design of C-RAN, when a large number of RRHs is deployed, the selection of RRH or user would be of salient importance considering the increased circuit power consumption of the RRHs. Hence, to enhance the quality-of-service while keeping the design more energy-efficient, the work in [14]–[16] focuses on joint RRH selection and beamforming vector optimization relying on mixed-integer non-linear programming (MINLP). More recently, Pan *et al.* [17] proposed a joint precoding and RRH selection to minimize the network power consumption, where both the RRHs and users have multiple antennas and each user is served by its nearby RRHs.

Against this background, our contributions are summarized as follows:

- *We propose an adaptive array design for hybrid beamforming in mmWave communication that adapts the architecture as well as the digital precoding depending on whether the channel is of line-of-sight (LOS) or non-line-of-sight (NLOS) nature. Explicitly, we design an adaptive array based architecture, where the array is fully-connected in LOS channel with an antenna spacing of $\lambda/2$, where λ is the wavelength. By contrast, in NLOS channels the sub-array-connected architecture is employed, where the antenna array is partitioned into sub-arrays with a sufficiently large separation so that each sub-array experiences independent fading to attain both beamforming and diversity gains. Furthermore, we demonstrate by simulation results that in LOS channels the digital transmit precoder (TPC) does not provide any performance advantage, since the RF beamformer alone captures potential performance improvements.*
- *We utilize the novel adaptive array design to propose an adaptive virtual cell formation in the PHY layer of C-RAN for mmWave hybrid beamforming aided systems, since the dynamic selection of RRHs is similar to a mmWave transmitter that adaptively switch between the fully-connected and ASA designs. In virtual cell formation, the user may maintain its connection with one or two RRH(s) depending on our proposed design criterion. We first present an algorithm for virtual cell formation for a single mobile user, where the RRHs connected to the user experience different channel conditions (LOS/NLOS). Then we extend our algorithm to a multi-user scenario, where the mobile users are distributed randomly and experience different channel conditions (LOS/NLOS) with the RRHs. Moreover, given the fronthaul constraints in C-RAN, for multi-user setting, we consider the maximum number of users that can be supported by the fronthaul link.*

The rest of the paper is organized as follows. Sec. II discusses the system model of our adaptive design, while Sec. III presents the adaptive array design conceived in this paper, followed by our numerical results. In Sec. IV, an adaptive virtual cell formation is proposed for C-RAN in mmWave communications as an extension of the adaptive array discussed in Sec. III. Finally, our conclusions are presented in Sec. V.

Notations: We use upper case boldface, $\mathbf{A}$, for matrices and lower case boldface, $\mathbf{a}$, for vectors. We use T, H for transpose, Hermitian transpose, respectively, while $\mathbb{E}$ denotes the expectation operation. Finally, we use $\mathcal{CN}$, $\mathcal{U}$, and i.i.d. to denote complex-valued normal distribution, uniform distribution, and independent and identical distribution, respectively.

II. System Model

In this section, we first commence by introducing the top-level view of network followed by the physical layer system design. In the considered network, N RRHs are connected to the CU through fronthaul interface and each RRH communicate with a user through wireless mmWave channel. Furthermore, each RRH is equipped with an antenna array to exploit beamforming gain owing to high propagation losses in mmWave channel. Additionally, each user can be connected to one or multiple RRHs to harness beamforming and diversity gains. Thus, a virtual cell with one or multiple RRH(s) is formed. Moreover, the architecture of each RRH can be fully-connected with its AEs [18], or can be a 2-sub-array-connected design with another RRH, which is described below by considering each design explicitly [19].

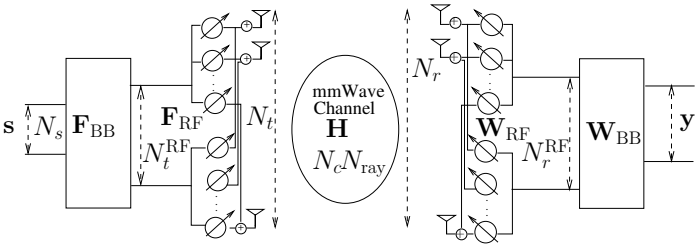

Fig. 2. *Fully-connected architecture.*

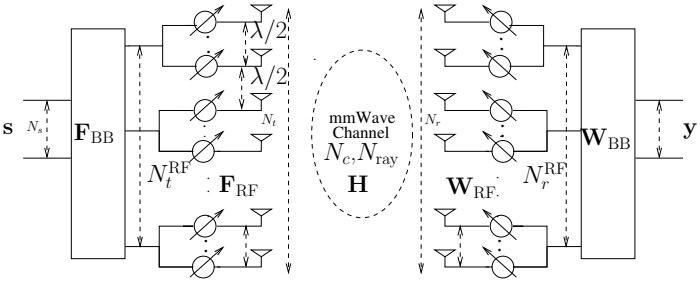

Fig. 3. *Sub-array-connected architecture.*

In the fully-connected design of Fig. 2, the antenna array is constructed by $\lambda/2$ spaced AEs, which are used for attaining beamforming gain required for compensating for the propagation losses. In this configuration, digital linear processing is performed using a TPC matrix $\mathbf{F}_{\mathrm{BB}}$ in the baseband, followed

by upconverting the signal to the carrier frequency as shown in Fig. 2. The upconverted signals are then phase-shifted using a beamformer matrix $\mathbf{F}_{\text{RF}}$ in the RF for directional transmission from the antennas. In this design, the phase shifters of all RF chains are connected to all the transmit antennas.

On the other hand, in the sub-array-connected design of Fig. 3, similar to the fully-connected design, the signals are digitally pre-processed using a TPC matrix $\mathbf{F}_{\text{BB}}$ in the baseband and then phase-shifted by employing a beamformer matrix $\mathbf{F}_{\text{RF}}$ in the RF for directional transmission. However, in contrast to the fully-connected design, the phase shifters are connected only to a subset of transmit antennas, which makes it both cost and energy efficient, since the number of phase shifters required per RF chain is smaller. Furthermore, we also note that the sub-arrays are closely spaced, typically at half-wavelength, and hence the channel of each sub-array will be correlated with that of the adjacent sub-array. By contrast, in the improved sub-array-connected design [18] of Fig. 4 (a), the antenna array is partitioned into sub-arrays, where each sub-array is spatially separated by a sufficiently large distance d, so that they experience independent fading. The advantage of partitioning the antenna array is that a beneficial diversity gain is obtained in addition to the beamforming gain. However, the additional diversity gain is obtained at the cost of a beamforming gain reduction due to splitting the array. Nevertheless, we have shown in [18] that the diversity gain obtained by partitioning exceeds the the beamforming gain reduction for our 2-sub-array-connected design shown in Fig. 4 (b) and hence the 2-sub-array-connected design achieves a better performance than the fully-connected design in terms of its rate for semi-correlated channels. Furthermore, we have also shown in [18] that further partitioning into more than 2-sub-arrays would degrade the performance. Hence, in this paper, we consider the *2-sub-array-connected* architecture as one of the constituent components for the adaptation. We note that each sub-array in the 2-sub-array-connected design may be fully-connected, as shown in Fig. 4 (b). In other words, each sub-array in Fig. 4(a) may have multiple RF chains to form a fully-connected design within the sub-array, as shown in Fig. 4(b).

Let us now consider a generic single-user mmWave hybrid MIMO system (fully-connected/sub-array-connected), where the transmitter is equipped with N_t antennas and the receiver with N_r antennas. Then the received signal vector after RF and baseband combining is given by

$$\mathbf{y} = \sqrt{P}\mathbf{W}_{\text{BB}}^H\mathbf{W}_{\text{RF}}^H\mathbf{H}\mathbf{F}_{\text{RF}}\mathbf{F}_{\text{BB}}\mathbf{s} + \mathbf{W}_{\text{BB}}^H\mathbf{W}_{\text{RF}}^H\mathbf{n}, \tag{1}$$

where $\mathbf{H}$ is the statistical channel model expressed as [20]:

$$\mathbf{H} = \sqrt{\frac{N_r N_t}{N_c N_{\text{ray}}}} \sum_{n_c=1}^{N_c} \sum_{n_{\text{ray}}=1}^{N_{\text{ray}}} \alpha_{n_c}^{n_{\text{ray}}} \mathbf{a}_r(\phi_{n_c}^{n_{\text{ray}}}) \mathbf{a}_t^T(\phi_{n_c}^{n_{\text{ray}}}). \tag{2}$$

The transmitter is equipped with N_t^{RF} chains and the receiver with N_r^{RF} chains, where $\mathbf{F}_{\text{RF}}$[1] is the RF beamformer matrix of size $N_t \times N_t^{\text{RF}}$, $\mathbf{F}_{\text{BB}}$ is the baseband TPC matrix of size $N_t^{\text{RF}} \times N_s$, $\mathbf{W}_{\text{RF}}^H$ is the RF combiner matrix of size $N_r^{\text{RF}} \times N_r$, and $\mathbf{W}_{\text{BB}}^H$ is the baseband combiner of size $N_s \times N_r^{\text{RF}}$. Furthermore, $\mathbf{y}$ is the $N_s \times 1$ received symbol vector, $\mathbf{s}$ is the symbol vector of size $N_s \times 1$, where $N_s \leq N_t^{\text{RF}}$ and $\mathbf{n}$ is the noise vector of i.i.d. associated with $\mathcal{CN}(0, \sigma^2)$, while $\mathbf{H}$ is the statistical channel matrix of size $N_r \times N_t$ so that $\mathbb{E}[\|\mathbf{H}\|_F^2] = N_t N_r$ in full-array configuration of Fig. 2 and for the 2-sub-array connection of Fig. 4, $\mathbf{H}$ is of size $N_r \times N_t$ and it is expressed as $\mathbf{H} = [\mathbf{H}_1\ \mathbf{H}_2]$, where $\mathbf{H}_1$ and $\mathbf{H}_2$ denote the sub-channel matrices. To elaborate further, $\alpha_{n_c}^{n_{\text{ray}}} \sim \mathcal{CN}(0,1)$ is a complex-valued Gaussian random variable, whose amplitude and phase are Rayleigh and uniform distributed, respectively, in a NLOS channel, while we have $\alpha = 1$ in a LOS channel, where $n_c = 1$, and $n_{\text{ray}} = 1$. For a uniform linear array (ULA) with N_r and N_t AEs, the response vectors $\mathbf{a}_r$ and $\mathbf{a}_t$ are expressed as:

$$\mathbf{a}_r(\phi_r) = [1\ e^{j\frac{2\pi}{\lambda}d\cos(\phi_r)} \dots e^{j\frac{2\pi}{\lambda}(N_r-1)d\cos(\phi_r)}]^T, \tag{3}$$

$$\mathbf{a}_t(\phi_t) = [1\ e^{j\frac{2\pi}{\lambda}d\cos(\phi_t)} \dots e^{j\frac{2\pi}{\lambda}(N_t-1)d\cos(\phi_t)}]^T, \tag{4}$$

where ϕ_r and ϕ_t are the angle of arrival and angle of departures, respectively. Finally, N_c and N_{ray} are the number of channel impulse response (CIR) clusters and rays, respectively.

Although a ULA is assumed in the paper, a uniform planar array (UPA) can also be adopted. For a UPA in the yz plane with W and H elements on the y and z axes respectively, the array response vector is given by:

$$\mathbf{a}(\phi,\theta) = \frac{1}{\sqrt{N}}([1, \dots, \exp^{jkd(m\sin(\phi)\sin(\theta)+n\cos(\theta))}, \dots, \dots, \exp^{jkd((W-1)\sin(\phi)\sin(\theta)+(H-1)\cos(\theta)}])^T, \tag{5}$$

where ϕ, θ denote the azimuthal and elevation angles, respectively.

In hybrid beamforming transmission, the signals are linearly precoded in the baseband, which is termed as transmit digital precoding (TPC), followed by analog RF beamforming, which is carried out in the RF stage, where the beamformer weights are designed for ensuring that the signal is steered in the direction of the desired user. This is explicitly captured in (1), where $\mathbf{F}_{\text{RF}}$ and $\mathbf{W}_{\text{RF}}$ are used for analog beamforming in the RF stage, while $\mathbf{F}_{\text{BB}}$ and $\mathbf{W}_{\text{BB}}$ are used for mitigating the inter-stream interference in the baseband.

Given this system model, the achievable rate in bits per second per Hertz (bps/Hz) before combining at the receiver is given by:

$$C = \mathbb{E}_{\mathbf{H}}\left[\log_2 \det\left(\mathbf{I}_{N_s} + \frac{P}{N_s N_\circ}\mathbf{F}_{\text{BB}}^H\mathbf{F}_{\text{RF}}^H\mathbf{H}^H\mathbf{H}\mathbf{F}_{\text{RF}}\mathbf{F}_{\text{BB}}\right)\right], \tag{6}$$

where P and $N_\circ$ are the signal and noise powers, respectively.

In the next section, we discuss the adaptive system design using the aforementioned architectures.

III. Adaptive System Design

The proposed system can be adapted at two levels. The first level of the adaptation focuses on transmitter hybrid architecture design which is based on whether the channel is of LOS or NLOS nature, and the second level of the adaptation is based on the hybrid precoding employed.

[1]Note that for sub-array-connected architecture, the matrix $\mathbf{F}_{\text{RF}}$ is diagonal. For further exposition on the structure of $\mathbf{F}_{\text{RF}}$ matrix for different architectures, we refer readers to [18].

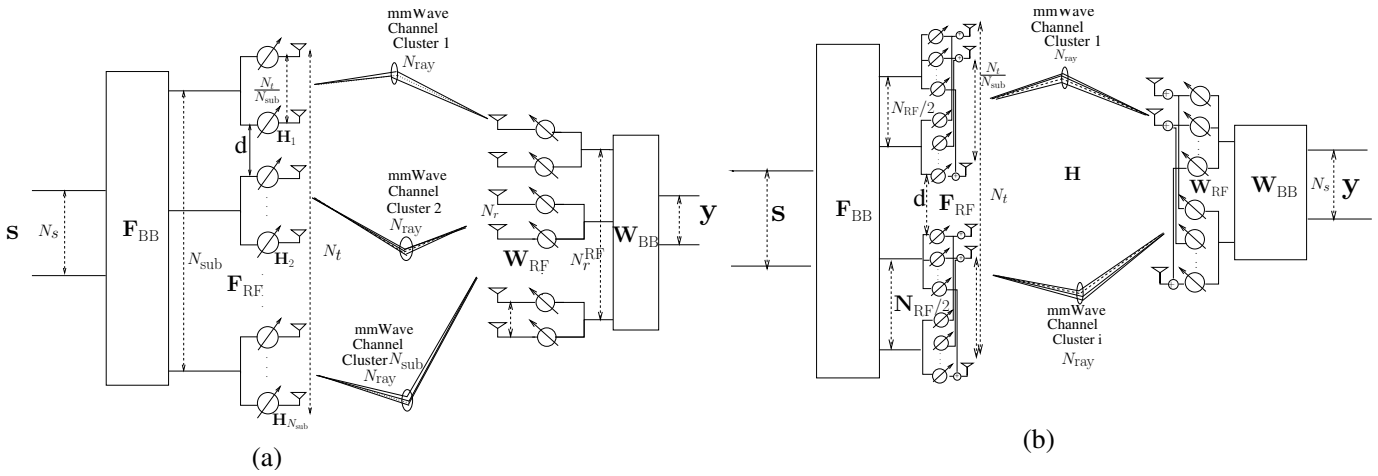

Fig. 4. *Sub-array-connected architecture — (a) Array of sub-array-connected architecture, where the separation d between two adjacent sub-arrays is sufficiently large so that each sub-array experiences independent fading (b) 2-sub-array-connected with multiple RF chains in each sub-array.*

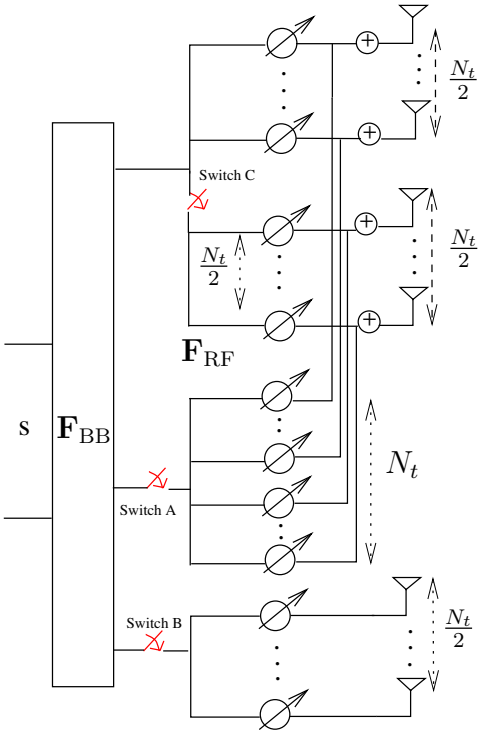

Fig. 5. *Adaptive array design, where switches A and C are activated to employ the fully-connected array in LOS channel conditions, while only switch B is activated to employ the 2-sub-array-connected array in NLOS channel conditions so as to attain both diversity and BF gains.*

The LOS channels exhibit a single dominant path, hence they have a single degree of freedom for signal transmission. Thus, the channel is devoid of any multiplexing/diversity gains that can be obtained at the transmitter/receiver.

On the other hand, the NLOS channels offer multiple degrees of freedom due to the rich scattering environment. As a benefit in NLOS channel conditions, the transmitter can achieve multiplexing/diversity gains.

In this paper, the adaptation is discussed at two levels: one in array design, and the other in hybrid precoding. In the first level of adaptation, we switch between the two array designs, namely fully-connected and 2-sub-array-connected. The rationale for choosing only these two designs is that fully-connected design provides full BF gain, while the 2-sub-array-connected design provides both diversity and BF gains. We have shown in [18] that having more than 2-sub-array-connected design degrades the performance in terms of achievable rate, because of the diminishing returns of the diversity gain, which hardly compensates for the reduction in the BF gain caused by splitting the antenna array. Therefore, we have decided to adapt between these two specific architectures.

First level of adaptation: The first level of adaptation is between the two choices of fully-connected and 2-sub-array-connected designs. Fig. 5 shows the adaptive array design equipped with switches A, B and C in order to facilitate both fully-connected and 2-sub-array-connected designs. It is instructive to note that although the transmitter in Fig. 5 is equipped with $3N_t/2$ AEs to facilitate both designs, only N_t AEs are used at any given time. In other words, the design of Fig. 5 is an amalgamation of both Fig. 2 and Fig. 4. Therefore, to employ the fully-connected design, switches A and C are activated to form a full antenna array having N_t AEs. By contrast, only switch B is activated to employ the 2-sub-array-connected design, where the top sub-array associated with $N_t/2$ AEs and the bottom sub-array with $N_t/2$ AEs are the constituent components of the design. More explicitly, to activate the fully-connected design, switches A and C are turned on while switch B is off. On the other hand, to activate the 2-sub-array-connected design, switch B is turned on while switches A and C are off.

To illustrate Fig. 5 in detail, let us consider an example, where the channel is of NLOS nature. In this setting, it was shown in [18] that having a 2-sub-array-connected design would provide better performance in terms of the achievable rate, because this design is capable of exploiting the diversity gain of the spatial degrees of freedom available from the

channel as well as the BF gain of $N_t/2$ derived from the antenna array within the sub-array. This is achieved in Fig. 5 by activating switch B only, where the transmitter now behaves as a 2-sub-array-connected scheme with $N_t/2$ AEs in each sub-array. By contrast, when the channel is of LOS in nature, there is only an angular degree of freedom, since the signal arriving from the sub-arrays impinge at the receiver at different angles of arrival, which is deprived of the additional spatial diversity gain obtained in NLOS channel conditions. Hence, we employ the fully-connected design, where we aim for achieving the full BF gain of N_t. This is achieved in Fig. 5 by activating the switches A and C while turning the switch B off.

Therefore, upon determining the channel conditions relying on Kurtosis-based LOS/NLOS identification method of [21], the receiver relays the information concerning the LOS/NLOS flag to the transmitter, which in turn then adapts to the array design according to the channel conditions. It is instructive to note that this adaptive design finds applications where the users are distributed in a way that some of them experience LOS and others NLOS channel. The transmitter adapts its array accordingly to improve the throughput of the LOS/NLOS users, as it will be shown later in Fig. 8.

Second level of adaptation: The second level of adaptation is employed in the hybrid precoding. In LOS channels, using analog beamforming at the RF stage is sufficient to capture the dominant LOS paths, as it will be shown in Fig. 7 and any digital precoder in the baseband would be redundant, since no multiplexing gain can be achieved in LOS channels. Hence, when the array is fully-connected in LOS channels, only analog beamforming is employed and the baseband TPC is chosen as the identity matrix, where virtually no signal processing is carried out.

By contrast, when the 2-sub-array-connected array is used in NLOS channels, employing analog RF beamforming and baseband precoding is preferred, as it will be shown in Fig. 6. This is because the NLOS channel provides multiplexing/diversity gains, which analog beamforming alone fails to capture effectively owing to the limitations of the analog phase shifters. Hence, baseband precoding is applied in addition to the analog RF beamforming to achieve the multiplexing/diversity gains in NLOS channels.

To characterize the performance of the constituent array designs in hybrid beamforming, we employ the following hybrid precoding[2]

1) *DFT-MUB:* In this configuration, we employ a discrete Fourier transform (DFT) aided beamformer for analog RF beamforming (ABF) [18], [19], where the beamformer weights are chosen from the DFT matrix. More explicitly, the columns of the ABF matrix $\mathbf{F}_{\text{RF}}$ are chosen from the DFT matrix which exhibit maximum correlation with the right singular vectors of the channel matrix $\mathbf{H}$, and the columns of the ABF matrix $\mathbf{W}_{\text{RF}}$ are chosen from the DFT matrix which exhibit maximum correlation with the left singular vectors of the channel matrix $\mathbf{H}$.
   On the other hand, the digital TPC matrix $\mathbf{F}_{\text{BB}}$ is chosen from a codebook constructed from the mutually unbiased bases (MUB). More explicitly, the specific TPC matrix is selected from the codebook which maximize the minimum SNR of the effective channel matrix $\mathbf{H}_{\text{eff}} = \mathbf{W}_{\text{RF}}^H \mathbf{H} \mathbf{F}_{\text{RF}}$. A more detailed mathematical analysis is presented in [18], [19]. The digital combiner matrix $\mathbf{W}_{\text{BB}}$ is chosen as the linear minimum mean squared error (LMMSE) solution.
2) *DFT-Identity:* Similar to the DFT-MUB hybrid precoding, we employ DFT assisted beamforming in the RF stage for both ABF matrices. However, for the baseband digital TPC an identity matrix is selected, where the first N_s columns of the identity matrix are chosen as the TPC weights. In other words, in this scenario there is virtually no digital processing of the signals in the baseband.

We will first analyze all the possible combinations of the array design with the aforementioned beamforming methods both in LOS and NLOS channel conditions. All the combinations of the array designs, the hybrid precoding and channel conditions are summarized in Table I.

TABLE I. *Combinations of array configuration and hybrid precoding designs.*

Array Design	*Channel*	*Hybrid Precoding*
Fully-connected	NLOS	DFT-MUB (ABF-TPC)
Fully-connected	NLOS	DFT-Identity (ABF-Identity)
Fully-connected	LOS	DFT-MUB (ABF-TPC)
Fully-connected	LOS	DFT-Identity (ABF-Identity)
2-sub-array-connected	NLOS	DFT-MUB (ABF-TPC)
2-sub-array-connected	NLOS	DFT-Identity (ABF-Identity)
2-sub-array-connected	LOS	DFT-MUB (ABF-TPC)
2-sub-array-connected	LOS	DFT-Identity (ABF-Identity)

The performance and achievable rate of all the combinations are shown in Fig. 6 and Fig. 7 for NLOS and LOS channels, respectively. The system configuration and parameters, such as the number of antennas, number of RF chains and modulation scheme are shown in Table II.

TABLE II. *System parameters.*

Parameters	*Values*
Modulation	4 QAM
N_t	64
N_r	16
N_t^{RF}	2
N_r^{RF}	2
N_s	1
N_{sub}	2
$\phi_{n_c}^{n_{\text{ray}}}$	$\mathcal{U}[0, 2\pi)$

Fig. 6 shows the achievable rate of a 64×16 MIMO in NLOS channel, when the DFT-MUB and DFT-Identity schemes are employed for the fully-connected as well as for the 2-sub-array-connected architectures. Fig. 6 shows that for both fully-connected and 2-sub-array-connected designs, the DFT-MUB outperforms the DFT-Identity based TPC in NLOS channel. This is because in NLOS conditions, where the channel is rich in spatial diversity, the ABF in the RF

[2]Note that any hybrid precoder combination that performs efficiently can be employed.

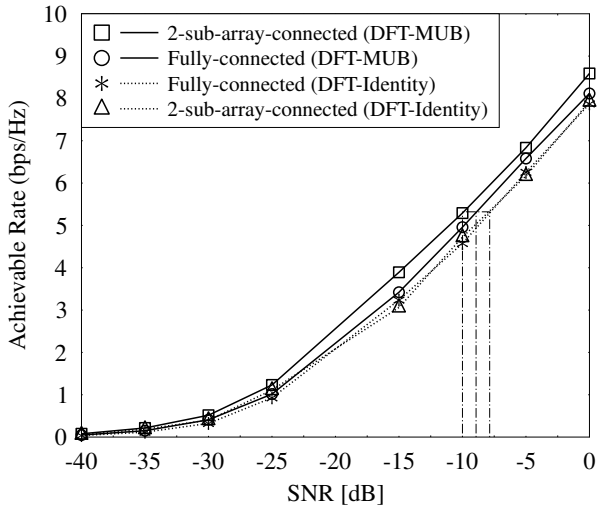

Fig. 6. *Achievable rate of* 64×16 *MIMO for the two designs with DFT-MUB (ABF-TPC) and DFT-Identity (ABF-Identity) in NLOS channel conditions, when* $N_t^{RF} = 4$ *and* $N_r^{RF} = 4$.

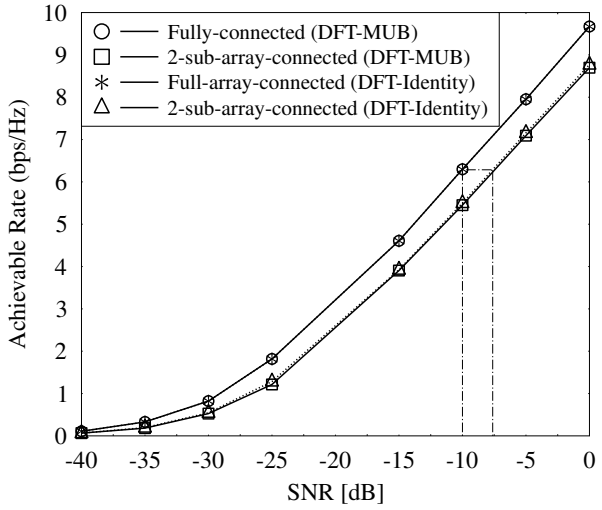

Fig. 7. *Achievable rate of* 64×16 *MIMO for the two designs with DFT-MUB (ABF-TPC) and DFT-Identity (ABF-Identity) in LOS channel conditions, when* $N_t^{RF} = 4$ *and* $N_r^{RF} = 4$.

stage fails to capture some of the spatial degrees of freedom, while the TPC can efficiently capture them. Furthermore, the 2-sub-array-connected design provides a better achievable rate than the fully-connected by a gain of around 1 dB in NLOS channels. This is due to the additional spatial diversity gain obtained from the spatially separated sub-arrays, which exceeds the loss in the beamforming gain [18].

Fig. 7 shows the achievable rate of a 64×16 MIMO in LOS channel condition when the DFT-MUB and DFT-Identity are employed for the two hybrid precoding architectures. It is seen in Fig. 6 that for both the fully-connected and 2-sub-array-connected designs, the achievable rate of DFT-MUB is similar to that of the DFT-Identity. This is because the ABF used in the RF stage can efficiently exploit the dominant path. Hence, employing TPC does not give any added advantage. Therefore, *any digital processing in the baseband is redundant in LOS channels*. Furthermore, it is also seen in Fig. 7 that in LOS channels, the fully-connected design is capable of providing a better rate than the 2-sub-array-connected design by about 2.5 dB gain. This is because we have no spatial diversity in LOS channels and thus it is more profitable to employ full-beamforming than partitioning the array into sub-arrays.

Based on the results shown in Fig. 6 and 7, of all the combinations listed in Table II, our adaptive design is configured to be fully-connected employing only ABF in LOS channels, and 2-sub-array-connected employing both ABF and TPC in NLOS channel conditions. In other words, in the scenario where the channel is of LOS nature, we employ carefully designed weights for ABF and choose the weights for the baseband TPC from an identity matrix. This is because the ABF alone captures the dominant LOS path. Hence, further digital processing of the signals using a TPC does not benefit us with any performance gain. Then, in the scenario where the channel is NLOS nature, we employ ABF-TPC, since the TPC is capable of capturing the degrees of freedom more efficiently. Table III shows the adaptation of the array design based on the channel conditions.

Thus, to leverage the diversity and beamforming gains accordingly to the channel conditions, the receiver determines the channel conditions relying on the Kurtosis-based LOS/NLOS identification method of [21] and feeds back the information flag to the transmitter over the feedback channel. Upon receiving this information, the transmitter adapts its array design and hybrid precoding accordingly.

Adaptive system results: Here we present simulation results for characterizing the performance of the fully-connected design, of the 2-sub-array connected design and of the adaptive design in both LOS and NLOS channels, where channel switches from LOS to NLOS with a probability of 0.5. We performed Monte Carlo simulations for analyzing the performance of the designs, when the ABF-TPC and ABF-Identity schemes are employed using the capacity equation in (5). The system configuration and parameters, such as the number of antennas, number of RF chains and modulation schemes are shown in Table II.

Fig. 8 shows the achievable rate of a 64×16 MIMO relying on the adaptive design, where the array switches to fully-connected relying on ABF-Identity precoding in LOS and to 2-sub-array-connected relying on ABF-TPC in NLOS conditions. The plot in Fig. 8 shows the achievable rate and performance benefits of adaptive design, of fully-connected design in all channel conditions, and of 2-sub-array-connected in all channel conditions, where the random channel label refers to either LOS/NLOS. It is seen in Fig. 8 that the adaptive

TABLE III. *Adaptive array configuration and hybrid precoding designs.*

Channel Condition	Array Design	Hybrid Precoding
LOS	Fully-connected	ABF-Identity
NLOS	2-sub-array-connected	ABF-TPC

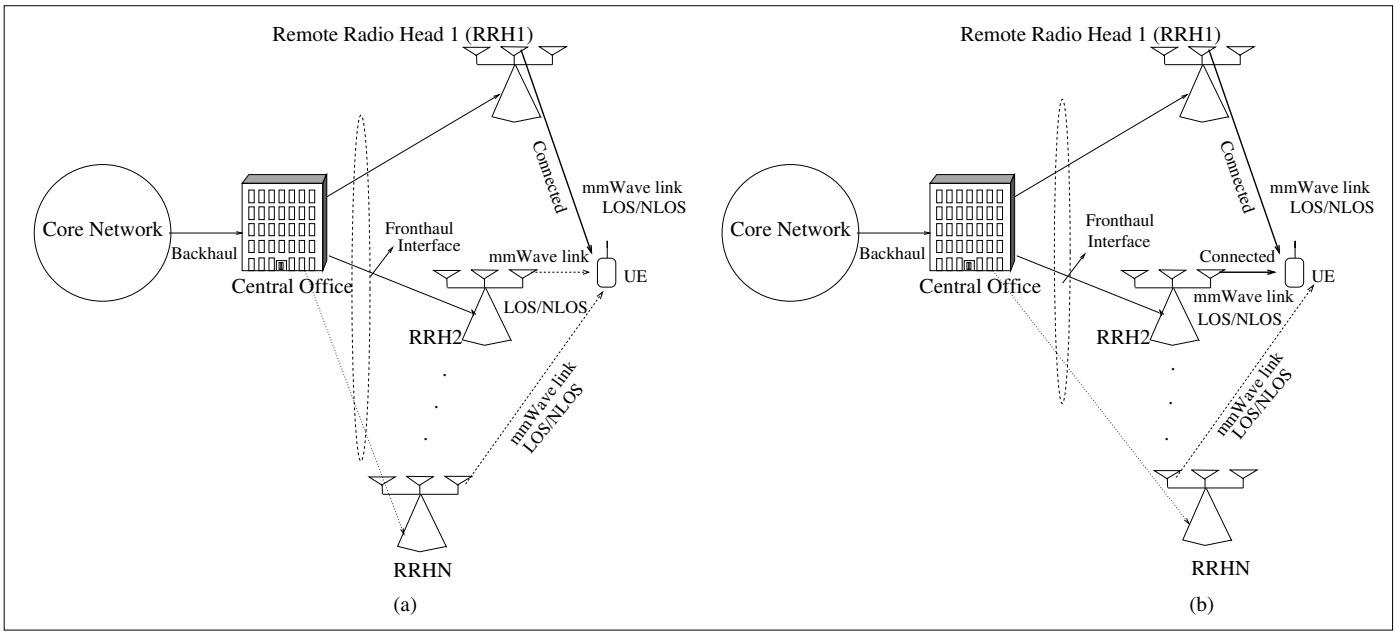

Fig. 9. *(a) RRH1 connected to user equipment (UE) using fully-connected design with N_t AEs. (b) Two RRHs connected to UE using fully-connected design with $N_t/2$ AEs on each to form a 2-sub-array-connected design.*

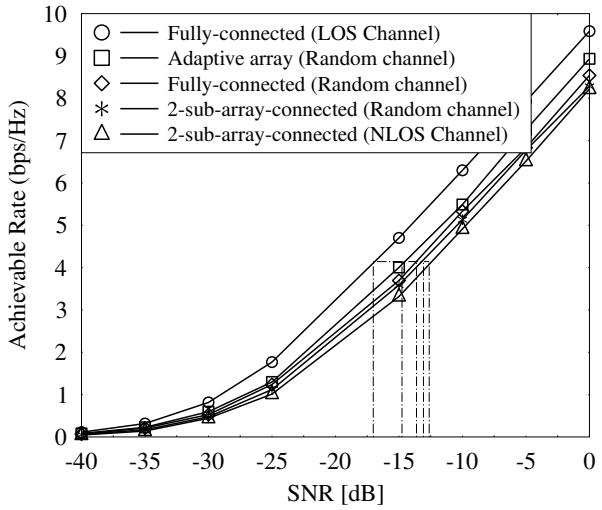

Fig. 8. *Achievable rate of 64×16 MIMO with adaptive design, where ABF-TPC is applied in NLOS and ABF-Identity is applied in LOS conditions. The channel is random since it varies between LOS and NLOS with probability 0.5.*

design achieves 1.5 dB gain against the fully-connected design and about 2 dB gain against the 2-sub-array-connected design, when the channel varies between LOS and NLOS.

In the next section, we discuss the aforementioned adaptive design in the context of C-RAN. We extend this analysis in the context of C-RAN, where a user can be connected to one RRH using fully-connected design or to two RRHs forming a 2-sub-array-connected design. The adaptation between these two design depends on the channel condition between the user and RRHs. A detailed explanation of the adaptive virtual cell formation in C-RAN is presented in the next section.

IV. Virtual Cell Formation in C-RAN

In this section, we utilize the adaptive array design for the physical layer design of C-RAN, where we assume that the total user load within the limited capacity of the fronthaul, in order to meet the finite capacity constraint imposed on the fronthaul [22]. Furthermore, the virtual cell formation here refers to the process where a mobile user connects to one or two RRH(s). As discussed in Sec. III, when the user is in the LOS channel condition, the transmitter employs fully-connected design, while when the user in the NLOS channel condition, the transmitter employs 2-sub-array connected design. In this paper, we relate this to C-RAN, where one or two RRH(s) are used to form fully-connected or 2-sub-array-connected designs. The rationale for strictly limiting the user connections with two RRHs is because of the performance degradation in terms of achievable rate when more than two RRHs are used for the user association with the same transmit power. A more detailed mathematical analysis is provided in [18].

In the context of the proposed architectures, a single RRH can connect with a user using the fully-connected architecture as shown in Fig. 9. In Fig. 9 (a), the user equipment may connect to RRH1, RRH2, . . ., RRHN according to the specific design criteria to be described in the next paragraph. Observe that RRH1 has been selected as the preferred RRH, where a fully-connected architecture is employed. Additionally, it is possible that two RRHs can form a virtual sub-array connected architecture as shown in Fig. 9 (b). Explicitly, as shown in Fig. 9 (b) RRH1 is coordinated with RRH2 to form a 2-sub-array-connected with $N_t/2$ AEs[3] in each RRH and forms a

[3]Note that the RRH always is fully-connected, however, the number of AEs to form the fully-connected design may vary in order to meet the transmit power constraint.

virtual cell with the UE as shown in Fig. 9 (b) with 2 bold lines from RRH1 and RRH2. More particularly, we propose a virtual cell formation algorithm for a single user, where the RRHs experience different channel conditions (LOS/NLOS), and the adaptive array design of the Sec. III is used while forming virtual cells. Then we extend our work to a multi-user environment, where the users are randomly distributed.

By acknowledging the challenges imposed on the fronthaul in C-RAN, such as its bandwidth, strict latency and jitter as well as the need for low cost transport network [23], in our proposed design we consider the maximum user load that can be supported by the fronthaul link. This corresponds to the total user load within the finite capacity of the fronthaul. However, to alleviate the fronthaul constraints, more effective signal processing techniques can be invoked to optimize the spectral efficiency, energy efficiency and delay, as in [24], [25]. Furthermore, to tackle the limited fronthaul capacity under heavy data traffic, techniques relying on sophisticated signal quantization and compression can be employed [26], [27]. Additionally, to deal with the dynamically fluctuating cell load and to enhance the C-RAN deployment, virtualization techniques such as software-defined-networking (SDN) [28] and network function virtualization (NFV) [29] can be used. Nevertheless, in this paper, we restrict our focus to PHY layer aspects of C-RAN. More particularly, we focus our attention on the virtual cell formation, where a mobile user can simultaneously connect to one or more than one RRH(s) [30]. Furthermore, in the case of multi-user scenarios, we consider the maximum number of users that can be supported in the fronthaul link.

It is instructive to note that, in our work, the digital TPC weight matrix $\mathbf{F}_{\text{BB}}$ discussed in Sec. III will be carried out at the CU, while the ABF weight matrix $\mathbf{F}_{\text{RF}}$ will be employed at the RRH, although the possible locations (RRH/CU) for computing the ABF and digital TPC matrices can be subsumed into four categories, which are: i) both ABF and TPC at the CU; ii) TPC at the CU and ABF at the RRH; iii) ABF at the CU and TPC at the RRH iv) both ABF and TPC at the RRH. However, in this paper, ABF is carried out at the RRH owing to the large overhead in relaying the channel matrix to the CU, especially in mmWave communications, since large antenna arrays would be employed. On the other hand, the digital TPC is designed relying on the effective channel matrix $\mathbf{H}_{\text{eff}}$ as discussed in Sec. III. Hence, overhead in relaying the effective channel matrix from the RRH to the CU would be low. Furthermore, since the baseband digital TPC is a joint signal processing for both RRHs, computing the TPC at the CU is an attractive solution.

A. Single User Cell Formation

Consider a single user that can be served by multiple RRHs, where the channel conditions between the user and each RRH can be classified as LOS and NLOS, as shown in Fig. 10.

In Fig. 10 each RRH is equipped with N_t AEs and the architecture of RRH can be either only fully-connected with N_t AEs or 2-sub-array-connected using two RRHs with each RRH using $N_t/2$ AEs, depending on the channel conditions. For the fully-connected design, all the N_t AEs are activated, while in the 2-sub-array-connected design only $N_t/2$ AEs are used in each RRH. It is instructive to note that N_t AEs can be employed for achieving better performance at the expense of a higher energy consumption. The algorithm of single user virtual cell formation is given in Algorithm 1 and the detailed exposition of the algorithm is presented below.

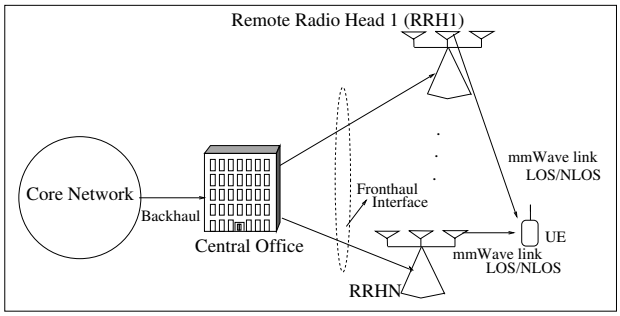

Fig. 10. *Single user served by two RRHs, where the channel between the user and each RRH can be either LOS or NLOS.*

Algorithm 1 Virtual Cell Formation for Single User

Categorize the RRHs into LOS and NLOS groups
Let LOS group has A RRHs and NLOS group has B DUs
For LOS group:
    Calculate the SNR for each link and sort the links in decreasing order as $\text{SNR}_{\text{L}_1} > \ldots > \text{SNR}_{\text{L}_\text{A}}$
For NLOS group:
    Calculate the SNR for each link and sort the links in decreasing order as $\text{SNR}_{\text{NL}_1} > \ldots > \text{SNR}_{\text{NL}_\text{B}}$
if $A > 0$ **then**
    if $\text{SNR}_{\text{NL}_1} - \text{SNR}_{\text{L}_1} <$ Threshold T **then**
        Form virtual cell by the RRH with associating SNR_{L_1}
    else
        Compute Capacities:
        C_1: Single RRH associated with SNR_{NL_1}
        C_2: Single RRH associated with SNR_{L_1}
        C_3: Dual-RRHs associated with SNR_{L_1} and SNR_{NL_1}
        C_4: Dual-RRHs associated with SNR_{NL_1} and SNR_{NL_2}
        C_5: Dual-RRHs associated with SNR_{L_1} and SNR_{L_2}
        Form virtual cell with link that has highest capacity i.e., $\max\{C_1, C_2, C_3, C_4, C_5\}$
    end if
else
    Compute Capacities:
    C_1: Single RRH associated with SNR_{NL_1}
    C_2: Dual-RRHs associated with SNR_{NL_1} and SNR_{NL_2}
    Form virtual cell with link that has highest capacity, i.e. $\max\{C_1, C_2\}$
end if

To better understand this, let us consider a scenario where there are N RRHs as shown in Fig. 9. In this setting, first

the CU categorizes the RRHs into LOS and NLOS groups, where the LOS group has A RRHs, whilst the NLOS group has B RRHs. Then the SNRs associated with the links in both LOS and NLOS groups are calculated for the user. If there are A>0 RRHs, select the specific RRH in LOS group having the highest SNR, say SNR_{L_1}, while selecting the two successive highest SNRs in NLOS, say SNR_{NL_1}, SNR_{NL_2}. Now the user can form a virtual cell with any of the three RRHs using a fully-connected architecture, or with two of the three RRHs using the 2-sub-array-connected architecture. Then we perform SNR comparison between the two links having the highest SNRs, i.e. SNR_{NL_1} and SNR_{L_1}. Then we compare (SNR_{NL_1} - SNR_{L_1}) to a predefined threshold T dB, which is calculated from Fig. 8. It is seen in Fig. 8 that the fully-connected design in LOS outperforms all other designs, in particular 2-sub-array-connected design by about 5 dB gain. Thus, in our case, T is set to 5 dB. So if (SNR_{NL_1} - SNR_{L_1}) ≤ 5, the virtual cell with RRH associated with the link SNR_{L_1} is formed. Otherwise, the CU computes the capacities of all the possible links, which are: (i) virtual cell capacity associated with SNR_{NL_1} using the fully-connected architecture; (ii) the virtual cell capacity associated with SNR_{L_1} using the fully-connected architecture; (iii) virtual cell capacity associated with SNR_{NL_1} and SNR_{L_1} forming the 2-sub-array-connected architecture using only $N_t/2$ AEs on each RRH; (iv) the virtual cell capacity associated with SNR_{NL_1} and SNR_{NL_2} forming 2-sub-array-connected architecture. After computing the capacities of all four cases, the CU forms the virtual cell with the link that has the highest capacity.

However, if there are no LOS groups, then the possible number of cases reduces to two, which are: (i) virtual cell capacity associated with SNR_{NL_1} using fully-connected architecture; (ii) virtual cell capacity associated with SNR_{NL_1} and SNR_{NL_2} forming the 2-sub-array-connected architecture. The CU then selects the link that has highest capacity.

For further understanding of the algorithm, let us consider the example shown in Fig. 9, where the channel between RRH1 and UE is NLOS and the channel between RRH2 and UE is LOS, and the channel between RRH3 and UE is NLOS. Furthermore, the SNR of RRH1>RRH2 and RRH3, and RRH2 is the highest SNR among all RRHs in LOS. In this setting, the possible cases for virtual cell formation are:
(i) cell with RRH1 serving UE with only fully-connected design as shown in Fig. 9, where RRH1 is connected to UE with N_t AEs;
(ii) cell with RRH2 serving UE with only fully-connected design, where RRH2 is connected to UE with N_t AEs;
(iii) cell with both RRH1 and RRH2 serving UE using the 2-sub-array-connected design as shown in Fig. 9 (b), where $N_t/2$ AEs are activated in each RRH;
(iv) cell with both RRH1 and RRH3 serving UE using 2-sub-array-connected design with $N_t/2$ AEs activated in each RRH.

From these possible cases, it is natural to associate UE with RRH1 using only the fully-connected design, regardless of LOS/NLOS owing to its higher SNR than with RRH2, or to form the 2-sub-array-connected design with RRH2 and RRH1 owing to NLOS conditions of RRH1 for diversity gains. However, it is seen in Fig. 6, that in NLOS conditions, the fully-connected design is inferior to the 2-sub-array-connected design. Furthermore, it is seen in Fig. 8 that the array with fully-connected design in LOS channel conditions outperforms the 2-sub-array-connected design by about 5 dB. This significant gain makes the problem interesting. In other words, although the link between RRH1 and UE, which is NLOS, has higher SNR than the SNR of the link between RRH2 and UE, which is LOS, associating UE to RRH2 achieves high rates as long as the gap between the SNRs is less than 5 dB. Furthermore, when the channel conditions in the link between RRH1 and UE as well as in the link between RRH2 and UE are NLOS, the possible cases for virtual cell formation are: (i) cell with RRH that has higher SNR to UE using fully-connected design or; (ii) cell with UE and collective RRHs to form the 2-sub-array-connected design. The CU computes capacities of all possible links and selects the link with the highest capacity.

On other hand, when the channel conditions in the links RRH1, RRH2 and RRH3 are LOS, the virtual cell associated with RRH that has a higher SNR is formed using the fully-connected design with N_t AEs. Thus, the adaptation between the architectures takes place according to the channel conditions and achievable rate. Table IV shows the summary of virtual cell formation of a single-user system of algorithm 1.

B. Multi-User Cell Formation

In this section, we discuss a multi-user scenario, where the users are randomly distributed and the channel between the RRHs and users can be either LOS or NLOS. Furthermore, each user can be associated with multiple RRHs either in LOS or NLOS and each RRH can be associated with multiple users, unlike in the single user case. However, as in the single user case, in the multi-user scenario, the CU computes the capacity of the links associated with the first two highest SNRs in both LOS and NLOS for each user and then forms the virtual cell for that user using the link which gives the highest capacity. This is repeated for all the users as shown in algorithm 2. It is instructive to note that given the finite capacity constraints in the fronthaul, we consider the maximum user load that can be supported. In other words, we allow the maximum number of users to communicate depending on the fronthaul capacity. Furthermore, the digital TPC weight matrix $\mathbf{F}_{\text{BB}}$ is applied at the CU, while the digitally precoded signals are phase shifted at the RRHs using $\mathbf{F}_{\text{RF}}$.

In a scenario, where two or more users having different channel conditions (LOS/NLOS) are associated with the same RRH, the transmitter activates fully-connected design with N_t AEs so as to satisfy all the users. For better illustration, let us consider an example shown in Fig. 11, where there are 2 RRHs as well as 2 users and let us consider the scenario where user 1 experiences LOS conditions associated with RRH1 and user 2 experiences NLOS propagation with both RRH1 and RRH2. In this setting, both RRHs will activate the fully-connected design. However, the RRH1 and the RRH2 transmit the signal to user 2 at half power. In other words, user 1 is served by RRH1 activating the fully-connected design to attain full BF gain, while user 2 is served both by RRH1 and RRH2, where

TABLE IV. *Virtual cell formation of a single-user in C-RAN.*

	Virtual Cell Formation	Conditions	
1	Single DU associated with SNR_{N1}	If number of LOS DUs $= 0$	Compute capacities of 1 and 2 and use the highest capacity
2	Dual-DUs associated with SNR_{N1} and SNR_{N1} with $N_{t/2}$ AEs in each DU		
1	Single DU associated with SNR_{N1}	If number of LOS DUs $=1$	Compute capacities of 1, 2, 3, 4 and use the highest capacity
2	Single DU associated with SNR_{L1}		
3	Dual-DUs associated with SNR_{L1} and SNR_{N1} using $N_{t/2}$ antennas on each DU		
4	Dual-DUs associated with SNR_{N1} and SNR_{N2} using $N_{t/2}$ antennas		
1	Single DU associated with SNR_{N1}	If number of LOS DUs >0	Compute capacities of 1, 2, 3, 4, 5 and use the highest capacity
2	Single DU associated with SNR_{L1}		
3	Dual-DUs associated with SNR_{L1} and SNR_{N1} using $N_{t/2}$ antennas on each DU		
4	Dual-DUs associated with SNR_{N1} and SNR_{N2} using $N_{t/2}$ antennas		
5	Dual-DUs associated with SNR_{L1} and SNR_{L2} using $N_{t/2}$ antennas		

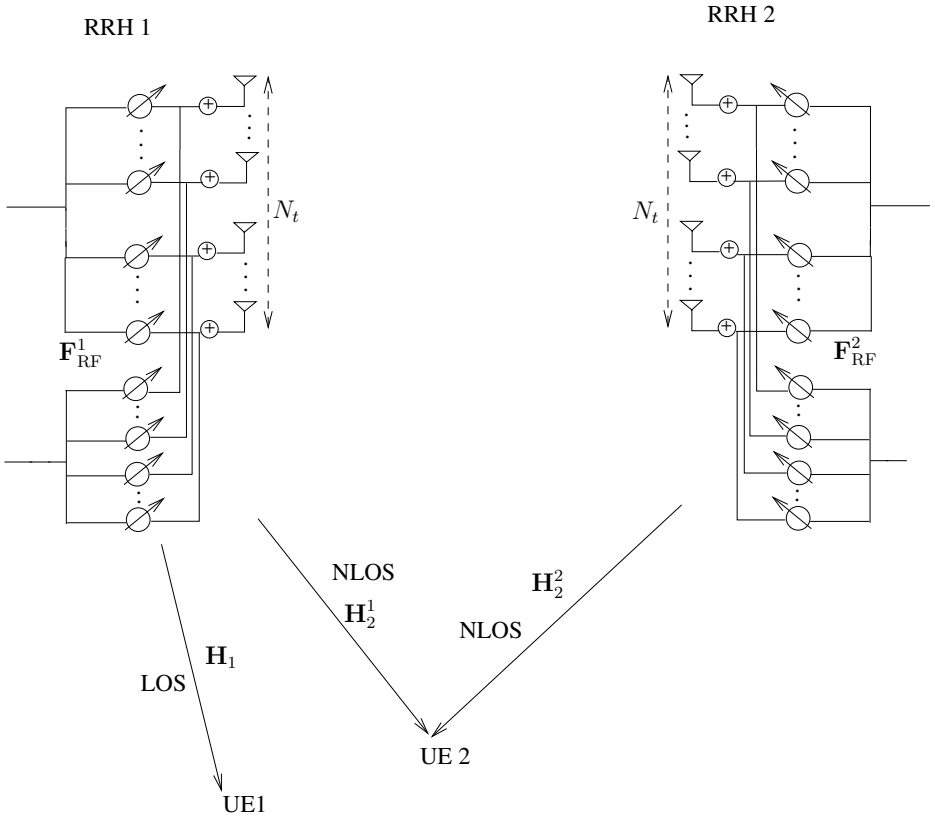

Fig. 11. *Example illustrating multiuser scenario, where a particular user is associated with 2 RRHs.*

each RRH uses fully-connected design and forms a 2-sub-array-connected design and each RRH transmits at half power. When combining the signal from the two RRHs, the receiver sees it as if it is transmitted from a transmitter associated with the 2-sub-array-connected design. Let us consider the example seen in Fig. 11, where the RRH1 employs the ABF $\mathbf{F}^1_{\text{RF}}$ and the RRH2 employs $\mathbf{F}^2_{\text{RF}}$, while the combined baseband digital TPC at the CU is $\mathbf{F_{BB}}$. Then the signal vector received at UE2 in the downlink before combining is given by

$$\mathbf{y}_{\text{UE2}} = \underbrace{\mathbf{H}^1_2\mathbf{F}^1_{\text{RF}}\mathbf{F_{BB}}\mathbf{x}_2 + \mathbf{H}^2_2\mathbf{F}^2_{\text{RF}}\mathbf{F_{BB}}\mathbf{x}_2}_{\text{desired signal}} + \underbrace{\mathbf{H}^1_2\mathbf{F}^1_{\text{RF}}\mathbf{F_{BB}}\mathbf{x}_1}_{\text{co-channel interference}} + \underbrace{\mathbf{n}}_{\text{noise}}. \tag{7}$$

In this way, an RRH can serve multiple users. The multi-user cell formation technique is given in algorithm 2. The exposition of Algorithm 2 is as follows: consider an N user system, and for each user the classification of the possible cases for virtual cell formation is carried out, as detailed for a single user. Furthermore, if the RRH has more than one

user for cell formation, i.e. if $N_{\text{RRH}} > 1$, then the RRH activates the fully-connected design for supporting multiple users. Otherwise, the RRH serves the users as required by the single user.

Algorithm 2 Virtual Cell Formation for Single User

For an N user system
for each user $n \in N$ **do**
    Repeat algorithm 1
end for
Let N_{RRH} be the number of users associated with a particular RRH
if $N_{\text{RRH}} > 1$ **then**
    Form virtual cell with N_t AEs as fully-connected architecture or forming a 2-sub-array-connected architecture with another RRH
else
    Form virtual cell with the number of antennas required by the single user.
end if

V. Conclusions

In this paper, we proposed an adaptive array design for hybrid beamforming in mmWave communications utilized in the context of virtual cell formation for PHY layer design of C-RAN. The adaption is performed at two levels depending on whether the channel is LOS or NLOS. The first level of adaptation takes place in the array design, while the second level of adaptation is employed in the hybrid precoding, where we demonstrated that the redundancy of the digital precoder in LOS channels. We showed using simulation results that the proposed adaptive design performs better than the fully-connected and sub-array-connected designs, when the channel varies between LOS and NLOS. Then we extended our proposed design to adaptive virtual cell formation for C-RAN systems in mmWave communications, where the channel between the RRH and the user equipment varies between LOS and NLOS.

References

[1] Rappaport *et al.*, "Millimeter wave mobile communications for 5G cellular: It will work!" *IEEE Access*, vol. 1, pp. 335–349, 2013.

[2] Y. Niu, Y. Li, D. Jin, L. Su, and A. V. Vasilakos, "A survey of millimeter wave (mmwave) communications for 5G: Opportunities and challenges," *CoRR*, vol. abs/1502.07228, 2015. [Online]. Available: http://arxiv.org/abs/1502.07228

[3] G. Maccartney, M. Samimi, and T. Rappaport, "Exploiting directionality for millimeter-wave wireless system improvement," in *Proc. ICC*, June 2015, pp. 2416–2422.

[4] A. Alkhateeb, J. Mo, N. Gonzlez-Prelcic, and R. W. Heath, "MIMO precoding and combining solutions for millimeter-wave systems," *IEEE Communications Magazine*, vol. 52, no. 12, pp. 122 – 131, 2014.

[5] A. Checko *et al.*, "Cloud RAN for mobile networks: A technology overview," *IEEE Commun. Surveys and Tutorials.*, vol. 17, no. 1, pp. 405–426, Firstquarter 2015.

[6] R. G. Stephen and R. Zhang, "Joint millimeter-wave fronthaul and OFDMA resource allocation in ultra-dense CRAN," *IEEE Trans. Commun.*, vol. 65, no. 3, pp. 1411–1423, March 2017.

[7] S. Han *et al.*, "Large-scale antenna systems with hybrid analog and digital beamforming for millimeter wave 5G," *IEEE Commun. Mag.*, vol. 53, no. 11, pp. 186–194, 2015.

[8] X. Gao *et al.*, "Energy-efficient hybrid analog and digital precoding for mmwave MIMO systems with large antenna arrays," *IEEE J. Sel. Areas Commun.*, vol. 34, no. 4, pp. 1499 – 1513, April 2016.

[9] M. Yilmaz, E. Guvenkaya, G. Mumcu, and H. Arslan, "Millimeter-wave wireless channel control using spatially adaptive antenna arrays," *IEEE Commun. Lett.*, vol. PP, no. 99, pp. 1–1, 2016.

[10] J. Song, J. Choi, S. G. Larew, D. J. Love, T. A. Thomas, and A. A. Ghosh, "Adaptive millimeter wave beam alignment for dual-polarized MIMO systems," *IEEE Trans. Wireless Commun.*, vol. 14, no. 11, pp. 6283–6296, Nov 2015.

[11] X. Huang, Y. J. Guo, and J. D. Bunton, "A hybrid adaptive antenna array," *IEEE Trans. Wireless Commun.*, vol. 9, no. 5, pp. 1770–1779, May 2010.

[12] A. Alkhateeb, O. E. Ayach, G. Leus, and R. W. Heath, "Single-sided adaptive estimation of multi-path millimeter wave channels," in *Proc. SPAWC*, June 2014, pp. 125–129.

[13] M. El-Hajjar, S. Zummo, and L. Hanzo, "Near-instantaneously adaptive cooperative uplink schemes based on space-time block codes and V-Blast," in *Proc. VTC*, April 2007, pp. 2200–2204.

[14] J. Tang, W. P. Tay, and T. Q. S. Quek, "Cross-layer resource allocation with elastic service scaling in cloud radio access network," *IEEE Trans. Wireless Commun.*, vol. 14, no. 9, pp. 5068–5081, Sept 2015.

[15] D. W. K. Ng and R. Schober, "Secure and green SWIPT in distributed antenna networks with limited backhaul capacity," *IEEE Trans. Wireless Commun.*, vol. 14, no. 9, pp. 5082–5097, Sept 2015.

[16] Y. Cheng, M. Pesavento, and A. Philipp, "Joint network optimization and downlink beamforming for CoMP transmissions using mixed integer conic programming," *IEEE Trans. Signal Process.*, vol. 61, no. 16, pp. 3972–3987, Aug 2013.

[17] C. Pan, H. Zhu, N. J. Gomes, and J. Wang, "Joint precoding and RRH selection for user-centric green MIMO C-RAN," *IEEE Trans. Wireless Commun.*, vol. 16, no. 5, pp. 2891–2906, May 2017.

[18] K. Satyanarayana, M. El-Hajjar, P. H. Kuo, A. Mourad, and L. Hanzo, "Dual-function hybrid beamforming and transmit diversity aided millimeter wave architecture," *IEEE Trans. Veh. Technol.*, vol. PP, no. 99, pp. 1–1, 2017.

[19] K. Satyanarayana, M. El-Hajjar, P.-H. Kuo, A. Mourad, and L. Hanzo, "Millimeter wave hybrid beamforming with DFT-MUB aided precoder codebook design," *Proc. VTC*, Sept. 2017.

[20] M. K. Samimi and T. S. Rappaport, "3-D millimeter-wave statistical channel model for 5G wireless system design," *IEEE Trans. Microw. Theory Tech.*, vol. 64, no. 7, pp. 2207–2225, July 2016.

[21] J. Zhang, J. Salmi, and E. S. Lohan, "Analysis of Kurtosis-based LOS/NLOS identification using indoor MIMO channel measurement," *IEEE Trans. Veh. Technol.*, vol. 62, no. 6, pp. 2871–2874, July 2013.

[22] M. Peng, C. Wang, V. Lau, and H. V. Poor, "Fronthaul-constrained cloud radio access networks: insights and challenges," *IEEE Wireless Commun.*, vol. 22, no. 2, pp. 152–160, April 2015.

[23] A. Checko, H. L. Christiansen, Y. Yan, L. Scolari, G. Kardaras, M. S. Berger, and L. Dittmann, "Cloud RAN for mobile networks — A technology overview," *IEEE Commun. Surveys and Tutorials.*, vol. 17, no. 1, pp. 405–426, Firstquarter 2015.

[24] J. Li, M. Peng, A. Cheng, Y. Yu, and C. Wang, "Resource allocation optimization for delay-sensitive traffic in fronthaul constrained cloud radio access networks," *IEEE Systems Journal*, vol. PP, no. 99, pp. 1–12, 2017.

[25] V. N. Ha, L. B. Le, and N. D. Oao, "Cooperative transmission in cloud RAN considering fronthaul capacity and cloud processing constraints," in *Proc. WCNC*, April 2014, pp. 1862–1867.

[26] L. Liu, S. Bi, and R. Zhang, "Joint power control and fronthaul rate allocation for throughput maximization in OFDMA-based cloud radio access network," *IEEE Trans. Commun.*, vol. 63, no. 11, pp. 4097–4110, Nov 2015.

[27] S. H. Park, O. Simeone, O. Sahin, and S. Shamai, "Joint decompression and decoding for cloud radio access networks," *IEEE Signal Process. Lett.*, vol. 20, no. 5, pp. 503–506, May 2013.

[28] A. Gudipati, D. Perry, L. E. Li, and S. Katti, "Softran: Software defined radio access network," in *in Proc. ACM SIGCOMM*. New York, NY, USA: ACM, 2013, pp. 25–30. [Online]. Available: http://doi.acm.org/10.1145/2491185.2491207

[29] NFV Working Group, "Network function virtualization — Introductory," in *white paper ETSI*, 2012.

[30] J. D. Bakker and R. Prasad, "Handover in a virtual cellular network," in *Proc. VTC*, vol. 1, 1999, pp. 544–548 vol.1.

K. Satyanarayana (www.satyanarayana.xyz) received his B. Tech. degree in Electrical Engineering from Indian Institute of Technology Madras, India, in 2014. During Jul'14-Aug'15, he worked as a research assistant at Indian Institute of Science, Bangalore. Currently, Satya is a research scholar in Wireless Communications at the University of Southampton in liaison with InterDigital Europe, London, UK. His research interests include millimeter wave communications, hybrid beamforming, with an emphasis on transceiver algorithms for wireless communication systems and multi-functional MIMO.

Mohammed El-Hajjar is an Associate Professor in the department of Electronics and Computer Science in the University of Southampton. He received his PhD in Wireless Communications from the University of Southampton, UK in 2008. Following the PhD, he joined Imagination Technologies as a design engineer, where he worked on designing and developing Imaginations multi-standard communications platform, which resulted in three patents. He is the recipient of several academic awards and has published a Wiley-IEEE book and in excess of 80 journal and conference papers. Mohammed's research interests include the design of intelligent and energy-efficient transceivers, MIMO, millimeter wave communications, cross-layer optimization for large-scale networks and Radio over fiber network design.

Ping-Heng Kuo is a staff engineer at InterDigital Europe, London, UK. He is currently involved in the European Horizon 2020 5G-PPP Phase-1 and Phase-2 projects including 5G-Crosshaul and 5G-Coral, as well as additional collaborative projects in the UK researching pre-standard radio access technologies for 5G and beyond. Prior to joining InterDigital in 2016, he has been a wireless communications technologies research engineer and a 3GPP RAN1 delegate at Industrial Technology Research Institute (ITRI) in Taiwan for 7 years, focusing on advanced physical layer technologies such as CoMP and Massive-MIMO schemes. Ping-Heng also held a visiting scholar position at Harvard University in 2014, and he has served as an editor of Industry Perspectives Column for IEEE Wireless Communications Magazine in 2015. He received his Ph. D. from University of Canterbury, New Zealand, and conducted an internship at Samsung Advanced Institute of Technology (SAIT) in Korea. Ping-Heng is the main inventor of 8 granted US patents and has authored more than 20 peer-reviewed conference/journal papers.

Alain A. M. Mourad holds a PhD degree in Telecommunications from ENST Bretagne in France. He has over 15 years experience in the wireless networks industry. He is currently leading the research and development of Next Generation Radio Access Networks at InterDigital International Labs (London, Berlin, Seoul). Prior to joining InterDigital, Dr. Mourad was a Principal Engineer at Samsung Electronics R&D (UK) and previously a Senior Engineer at Mitsubishi Electric R&D Centre Europe (France). Throughout his career, Dr. Mourad has been active in the research and standardization of recent communication networks (5G/4G/3G) and broadcasting systems (ATSC 3.0/DVB-NGH/DVB-T2). He has held various leadership roles in the industry, invented over 35 granted patents and several other patent applications, and authored over 50 peer-reviewed publications. He received the Inventor of the Year Award from Samsung Electronics R&D (UK) twice in 2012 and 2013, and in 2016 InterDigital Innovation Award for the idea, creation, and execution of InterDigital Europe.

Lajos Hanzo (http://www-mobile.ecs.soton.ac.uk) FREng, FIEEE, FIET, Fellow of EURASIP, DSc received his degree in electronics in 1976 and his doctorate in 1983. In 2009 he was awarded an honorary doctorate by the Technical University of Budapest and in 2015 by the University of Edinburgh. In 2016 he was admitted to the Hungarian Academy of Science. During his 40-year career in telecommunications he has held various research and academic posts in Hungary, Germany and the UK. Since 1986 he has been with the School of Electronics and Computer Science, University of Southampton, UK, where he holds the chair in telecommunications. He has successfully supervised 100+ PhD students, co-authored 18 John Wiley/IEEE Press books on mobile radio communications totalling in excess of 10 000 pages, published 1600+ research contributions at IEEE Xplore, acted both as TPC and General Chair of IEEE conferences, presented keynote lectures and has been awarded a number of distinctions. Currently he is directing a 60-strong academic research team, working on a range of research projects in the field of wireless multimedia communications sponsored by industry, the Engineering and Physical Sciences Research Council (EPSRC) UK, the European Research Councils Advanced Fellow Grant and the Royal Societys Wolfson Research Merit Award. He is an enthusiastic supporter of industrial and academic liaison and he offers a range of industrial courses. He is also a Governor of the IEEE VTS. During 2008 - 2012 he was the Editor-in-Chief of the IEEE Press and a Chaired Professor also at Tsinghua University, Beijing. For further information on research in progress and associated publications please refer to http://wwwmobile.ecs.soton.ac.uk Lajos has 30 000+ citations and an H-index of 68.